

promoting access to White Rose research papers



Universities of Leeds, Sheffield and York
<http://eprints.whiterose.ac.uk/>

This is an author produced version of a paper published in **Journal of Geophysical Research**.

White Rose Research Online URL for this paper:
<http://eprints.whiterose.ac.uk/9011/>

Published paper

Neil, S.P., Scourse, J.D., Bigg, G.R. and Uehara, K. (2009) *Changes in wave climate over the northwest European shelf seas during the last 12,000 years*. Journal of Geophysical Research (All Series), 114 . C06015.

**1 Changes in wave climate over the northwest
2 European shelf seas during the last 12,000 years**

S. P. Neill,¹ J. D. Scourse,¹ G. R. Bigg,² and K. Uehara³

S. P. Neill, School of Ocean Sciences, Bangor University, Marine Science Laboratories, Menai Bridge, LL59 5AB, UK. (s.p.neill@bangor.ac.uk)

J. D. Scourse, School of Ocean Sciences, Bangor University, Marine Science Laboratories, Menai Bridge, LL59 5AB, UK. (j.scourse@bangor.ac.uk)

G. R. Bigg, Department of Geography, The University of Sheffield, Sheffield, S10 2TN, UK. (grant.bigg@sheffield.ac.uk)

K. Uehara, Research Institute for Applied Mechanics, Kyushu University, Kasuga, Fukuoka 816-8580, Japan. (uehara@riam.kyushu-u.ac.jp)

¹School of Ocean Sciences, Bangor

3 **Abstract.** Due to depth-attenuation of wave orbital velocity, wave-induced
4 bed shear stress is much more sensitive to changes in total water depth than
5 tidal-induced bed shear stress. The ratio between wave- and tidal-induced
6 bed shear stress in many shelf sea regions has varied considerably over the
7 recent geological past due to combined eustatic changes in sea level and iso-
8 static adjustment. In order to capture the high frequency nature of wind events,
9 a two-dimensional spectral wave model is here applied at high temporal res-
10 olution to time slices from 12 ka BP to present using paleobathymetries of
11 the NW European shelf seas. By contrasting paleo wave climates and bed
12 shear stress distributions with present-day conditions the model results demon-
13 strate that, in regions of the shelf seas which remained wet continuously over
14 the last 12,000 years, annual root-mean-square (rms) and peak wave heights
15 increased from 12 ka BP to present. This increase in wave height was accom-

University, Marine Science Laboratories,
Menai Bridge, LL59 5AB, UK.

²Department of Geography, The
University of Sheffield, Sheffield, S10 2TN,
UK.

³Research Institute for Applied
Mechanics, Kyushu University, Kasuga,
Fukuoka 816-8580, Japan.

16 panied by a large reduction in the annual rms wave-induced bed shear stress,
17 primarily due to a reduction in the magnitude of wave orbital velocity pen-
18 etrating to the bed for increasing relative sea level. In regions of the shelf
19 seas which remained wet over the last 12,000 years, the annual mean ratio
20 of wave- to (M_2) tidal-induced bed shear stress decreased from 1 (at 12 ka
21 BP) to its present day value of 0.5. Therefore, compared to present-day con-
22 ditions, waves had a more important contribution to large-scale sediment trans-
23 port processes in the Celtic Sea and the northwestern North Sea at 12 ka BP.

1. Introduction

24 The repeated flooding and emersion of the continental shelves driven by Quaternary
25 glacio-eustatic cycles of up to 115 – 135 m [Milne *et al.*, 2002] has been described as
26 *... the most important geologic event of recent time ...* [Newell, 1961]. The areal extent
27 of the shelf seas (< 200 m deep) is now 425% greater than during the Last Glacial
28 Maximum (LGM), 7% of the total global sea-surface. The changes in relative sea level
29 over the last deglacial transition were largely driven by glacio-eustatic, glacio-isostatic and
30 ice-water gravitational attraction mechanisms [Mitrovica *et al.*, 2001], and had a profound
31 impact on the hydrodynamic evolution of the shelf seas. The tidal dynamic feedbacks,
32 with implications for tidal amplitudes, bed shear stress and sediment dynamics, are under
33 active investigation via geologically-constrained paleotidal models [Austin, 1991; Hinton,
34 1995, 1996; van der Molen and de Swart, 2001b; Uehara *et al.*, 2006; Rippeth *et al.*, 2008;
35 Scourse *et al.*, 2009]. Although tidal currents dominate long-term sediment movements
36 over shelf seas [Pingree and Griffiths, 1979], waves also have an important contribution
37 [e.g. Ogston and Sternberg, 1999; van der Molen, 2002]. Due to attenuation of wave motion
38 with depth, the magnitude of wave-induced bed shear stress (τ_w) is much more sensitive
39 to variations in total water depth, in contrast to tidal-induced bed shear stress (τ_0). For
40 example, a typical wave height of 3 m with wave period 8 s will result in a relatively high
41 bed shear stress of 2.02 N m⁻² in 20 m water depth, reducing to 0.37 N m⁻² in 50 m
42 water depth and 0.04 N m⁻² in 100 m water depth. Therefore, wave-induced bed shear
43 stresses have varied considerably from the Late-glacial to present, due to a corresponding
44 change in sea level and isostatic/eustatic adjustment over this time period [Peltier, 2002].

45 In addition, the astronomical tide-generating forces have been relatively constant over the
46 last 12,000 years [*Berger et al.*, 1992]. In contrast, wind climate, and hence the resulting
47 wave climate, has varied considerably over this period [*Renssen et al.*, 2007]. Indeed,
48 even within the decadal timescale of present-day wind conditions, there is considerable
49 inter-annual variability in wind (and resulting wave) climates [*Hurrell and van Loon*,
50 1997]. Consideration of wave-induced bed shear stress, in addition to tidal-induced bed
51 shear stress, provides a more accurate representation of net bed shear stress and hence
52 sediment transport processes in shelf seas. Further, wind waves are the dominant cause
53 of sediment entrainment in many regions of shelf seas with low tidal energy [e.g. *van der*
54 *Molen*, 2002] and, since wind forcing is independent of tides, generally accelerate the
55 magnitude of sediment transport and hence the rate of bed level change [*Vincent et al.*,
56 1998]. An estimate of how the ratio between wave- and tidal-induced bed shear stress at
57 shelf scale has varied since the Late-glacial provides a useful tool with which to analyze
58 bedforms and constrain the timing of sediment deposition events/regimes observed in
59 sediment cores recovered from shelf seas.

60 A simple point model, based on a binned time series wind climate applied to a JON-
61 SWAP spectrum, has been applied to paleo time slices of the southern North Sea, demon-
62 strating that mean wave heights in this region increased from 7.5 ka BP to present [*van der*
63 *Molen and de Swart*, 2001a]. Application of sediment transport formulae to wave model
64 output suggested that in this region (where present-day water depths are of order 30 – 50
65 m), the mode of wave-induced sediment transport changed from dominantly suspended
66 transport prior to 6 ka BP to dominantly bed-load transport thereafter, due to sea-level
67 rise. These simulations were made on the assumption that wind climate was invariant over

68 the Holocene, and neglected refraction and non-linear wave-wave interactions. As far as
69 the authors are aware, this is the only published work on paleowave modeling, particularly
70 with application to sediment transport processes over any region at shelf scale. Further,
71 neither inter-annual variability or annual estimates of mean and peak wave conditions at
72 shelf scale have been estimated for paleo time slices.

73 In this paper, a two-dimensional (2D) spectral wave model is applied to the NW Eu-
74 ropean shelf seas for a decade of wind-forcing at synoptic-scale variability. Initially, the
75 model is validated using present-day bathymetry, providing a benchmark for comparison
76 with subsequent paleo-simulations. The model is then applied to a series of paleobathyme-
77 tries from 12 ka BP to present. The degree of sensitivity of model results to bathymetry
78 or atmospheric forcing is tested by examining the response of the model at each time slice
79 to a wide inter-annual variability in the decade of predicted wave climates, ranging from
80 conditions representative in character of much colder climates to warmer climates than
81 present. Finally, bed shear stress output by the wave model for time slices from 12 ka BP
82 to present is contrasted with tidal-induced bed shear stress output from a paleotidal model
83 study of the same region [*Uehara et al.*, 2006]. The application of this work is to assist in
84 analysis of bedforms and constraining the timing of sediment deposition events/regimes
85 over the NW European shelf seas through the Late-glacial and Holocene.

2. Study Area

86 The NW European shelf seas are located on the northeastern margin of the North
87 Atlantic and are generally shallower than 200 m (Figure 1). The Celtic Sea, Malin Sea
88 and northern North Sea are exposed to Atlantic waters, with water depths in the range
89 100–200 m, with the exception of the deeper (600 m) Norwegian trench in the northeastern

90 North Sea. The Celtic Sea borders the Irish Sea to the north, a semi-enclosed water body
91 containing a north-south orientated channel of depth 250 m. To the east of the Celtic
92 Sea, the English Channel connects to the southern North Sea. This region of the North
93 Sea is generally shallower than 50 m, and contains various large sandbanks, the most
94 prominent of which is Dogger Bank. Substantial crustal rebound occurred over the NW
95 European continental shelf due to unloading of the local British and Fennoscandian ice
96 sheets [*Peltier, 1994; Lambeck, 1995*]. These ice sheets had ablated by 9 ka BP and
97 their deglaciation was a major source of sediment supply to the NW European shelf seas
98 [*Boulton et al., 1985; Cameron et al., 1987; Scourse et al., 2009*], with a significant role in
99 the formation of large sand banks such as Dogger Bank [*Carr et al., 2006*].

100 The climate of the NW European shelf is dominated by the polar front [*Palutikof et al.,*
101 *1997*]. The instability of this front causes depressions to form, tracking across the North
102 Atlantic and following a preferred route which passes between Iceland and Scotland. As
103 these depressions move across the Atlantic, they follow a life cycle which, by the time
104 they reach the British Isles, means that they are generally in a phase of maturity or
105 decay. There is considerable variation in the wind climate around the NW European
106 shelf seas, but the strongest winds generally emanate from the west and south, and the
107 mean winds from the southwest [*Barrow and Hulme, 1997*]. Wind speeds tend to be
108 highest to the northwest of the British Isles (closest to the depression tracks), decreasing
109 towards the south and east. An annual cycle of higher wind speeds in winter and lower
110 speeds in summer reflects the seasonally varying strength of the large-scale atmospheric
111 circulation [*Palutikof et al., 1997*]. Inter-annual variability in the synoptic-scale circulation
112 over the Atlantic is described by the North Atlantic Oscillation (NAO) index, which

113 exhibits considerable inter-annual variability. The strong background flow leads to high
114 mean wave energy over the shelf seas and the variability results in a wave climate with
115 considerable extremes [Draper, 1980]. In regions of the shelf seas exposed to the Atlantic,
116 the orbital velocity, and hence wave-induced bed shear stress, of the longer-period (swell)
117 waves penetrates to the sea bed. Where fetch length is sufficient, the wave distribution
118 over the shelf seas broadly follows the wind distribution [Draper, 1980]. Due to the
119 dominant southwesterly wind direction, many regions of the NW European shelf seas are
120 relatively sheltered from wind effects and hence experience relatively low wave energy,
121 particularly the western seaboard of the North Sea (sheltered by the UK land mass) and
122 the northern half of the Irish Sea (sheltered by Ireland).

3. Data

3.1. Bathymetry Data

123 The relative sea-level data were supplied by Kurt Lambeck every 1 ka from 12 ka BP to
124 present, based on a glacio-isostatic adjustment (GIA) model of Lambeck [1995], updated
125 to incorporate recent advances in ice-sheet modeling and crustal-rebound formulation [c.f.
126 Lambeck and Chappell, 2001; Lambeck and Purcell, 2001; Lambeck et al., 2003]. Since
127 glacio-isostatic (un)loading history can result in profound vertical crustal movement, in
128 particular over formerly glaciated continental shelves, this approach is more realistic than
129 assuming solely eustatic sea-level changes as in early tidal modeling experiments [e.g.
130 Austin, 1991].

131 Paleobathymetry data at each time slice were derived by combining the relative sea-
132 level information with a present-day bathymetry, defined on the same horizontal grid.
133 Grid resolution of the bathymetry time slices is $1/12^\circ$ in both latitude and longitude

134 (~ 7 km) and the domain extends from 15°W to 15°E and from 45°N to 65°N (Figure
135 1). Bathymetries for selected paleo time slices are plotted in Figure 2. The derivation of
136 the paleo and present-day bathymetry data are described in more detail in *Uehara et al.*
137 [2006].

3.2. Wind Data

138 The source of synoptic surface wind fields was the ECMWF-ERA-Interim reanalysis
139 [*Simmons et al.*, 2006], available at a (global) grid resolution of 1.5° , with a time step of
140 3-hours from 1989-1998, a decade which witnessed considerable variability in the NAO
141 (Table 1), and hence considerable inter-annual variability with which to examine extremes
142 in the wave model. The ECMWF-ERA-Interim analysis differs from previous reanalysis
143 products (i.e. ERA-15 and ERA-40) in that it includes 4D-Var (or data assimilation in
144 time as well as all three spatial dimensions) and has improved horizontal resolution (T255
145 ~ 80 km in contrast to T159 ~ 125 km for ERA-40). The data available to the user
146 is at a similar resolution to the previous ERA-40 and ERA-15 datasets, but the original
147 analysis is at a better resolution, hence the standard gridpoint data should represent the
148 observed atmosphere better. For present-day validation of the wave model, one year of
149 wind data was obtained from six meteorological stations, each in relative proximity to
150 six corresponding waveriders (Table 2). In situ wind data were used for the validation
151 exercise in order to resolve more accurately the high frequency (generally half-hourly) wave
152 observations (section 3.3). The wind data is hourly (2007) for five of the meteorological
153 stations (Crosby, Milford Haven, Isle of Portland, Wattisham, and Loftus) and 3-hourly
154 (1975) for the station located furthest offshore (Stevenson).

3.3. Wave Data

155 For present-day validation of the wave model, time series of significant wave height
156 (H_s) and peak wave period (T_p) were obtained from five CEFAS directional waveriders in
157 regions of varying wave exposure and water depth (Table 2). These data were available
158 for the entire year 2007 at a sampling frequency of 2 h^{-1} . In addition, 3-hourly wave data
159 for 1975 were obtained from a non-directional UK Met Office waverider located further
160 offshore (Stevenson). The locations of the wave buoys are plotted on Figure 1.

4. Modeling

161 A spectral wave model was used to calculate the present-day and paleo wave cli-
162 mates over the NW European shelf seas. The key model inputs were wind forcing and
163 bathymetry. The wave model was applied at the same spatial resolution as the bathymetry
164 data ($1/12^\circ$) for time slices from 12 ka BP until present. For the maximum wind speed
165 considered (30 m s^{-1}), the fetch length for a fully developed sea, based on a JONSWAP
166 spectrum [Carter, 1982], is 400 km. Hence, although full bathymetric domains were used
167 for the wave simulations, only results $> 400 \text{ km}$ from the model boundaries were analyzed
168 (Figure 1). Depending on wind speed, waves within this 400 km ‘buffer zone’ adjacent to
169 the model boundary may be erroneously fetch-limited when waves are propagating from
170 the direction of an open boundary.

4.1. Model Description

171 SWAN (Simulating WAVes Nearshore) is an Eulerian formulation of the discrete wave
172 action balance equation [Booij *et al.*, 1999]. The model is spectrally discrete in frequencies
173 and directions, and the kinematic behavior of the waves is described with the linear theory

174 of gravity waves. The deep water physics of SWAN are taken from the WAM model
 175 [*Komen et al.*, 1994]. The model also includes shallow-water physics, namely bottom
 176 friction, refraction and shoaling. SWAN has two modes: stationary and non-stationary.
 177 Non-stationary mode is time-dependent, hence the evolution of the wave field can be
 178 modeled realistically, using boundary conditions of time-varying wind speed and direction
 179 [e.g. *Ris et al.*, 1999; *Neill et al.*, 2007]. This is, however, computationally expensive since
 180 a time step much smaller than the wind forcing time step is required for stability. In order
 181 to capture the high frequency nature of wind events, wave simulations at high temporal
 182 resolution were required for several time slices of the NW European shelf seas. Since
 183 the length of simulations was a decade, a more economical method was required. This
 184 involved running SWAN in stationary (steady state) mode.

185 In stationary mode, the evolution of the action density N is governed by the time-
 186 independent wave action balance equation [*Booij et al.*, 1999]

$$187 \quad \frac{\partial}{\partial x} c_x N + \frac{\partial}{\partial y} c_y N + \frac{\partial}{\partial \sigma} c_\sigma N + \frac{\partial}{\partial \theta} c_\theta N = \frac{S}{\sigma} \quad (1)$$

188 where c_x and c_y are the propagation velocities in the x and y directions, σ is frequency,
 189 θ is wave direction and S represents the source terms, i.e. generation, dissipation, and
 190 non-linear wave-wave interactions. For this application, the wave energy spectrum at each
 191 grid point was divided into 40 frequency components and 45 direction components. The
 192 lowest model frequency was 0.05 s^{-1} (period $T = 20 \text{ s}$, wavelength $L = 625 \text{ m}$), and the
 193 highest frequency resolved by the model was 2 s^{-1} ($T = 0.5 \text{ s}$, $L = 0.4 \text{ m}$). The effect of
 194 waves at higher frequencies was included in the calculation of the source terms.

195 For each cell of the model grid, a matrix of significant wave height (H_s), peak wave
 196 period (T_p), and the root-mean-square-value of orbital velocity near the bed (U_{rms}) was

197 produced as a lookup table using a discrete range of wind speeds and directions held
198 constant over the entire model domain. From a consideration of the wind climate over
199 the NW European shelf, a suitable range of discrete wind direction and speed bins was
200 selected as $\theta = 0, 15, \dots, 345^\circ$ and $W_r = 2, 4, \dots, 30 \text{ m s}^{-1}$ respectively (i.e. $24 \times 15 = 360$
201 simulations) [Neill *et al.*, 2008]. The final products of the model (time series of H_s , T_p ,
202 and U_{rms}) were derived by applying actual wind data to the lookup tables.

4.2. Model Validation

203 The wave model was validated with data of H_s and T_p from five wave buoys distributed
204 around the UK coastline (Figure 1, Table 2). Simulations were made for an entire year
205 (2007), using hourly wind data from meteorological stations close to each wave buoy
206 applied to the lookup tables. To determine model performance further offshore, the same
207 comparison was made at a wave buoy located in deeper water (160 m), 3-hourly throughout
208 1975. The model has captured much of the detail throughout the year in terms of the
209 magnitude and phase of H_s at all six stations (Figure 3). Probability density plots of
210 modeled and observed H_s (Figure 5) demonstrate good model performance at two of the
211 stations (Liverpool Bay and Poole Bay) and reasonable performance at the other four
212 stations. The model performs less satisfactorily when comparing with observed values of
213 T_p (Figure 4). The model often under-predicts T_p (Figure 6), mainly due to an absence
214 of swell waves in the rapid calculation method, since the model has not been nested
215 within a larger area model of the North Atlantic [e.g. Elliott and Neill, 2007]. For such a
216 rapid calculation method, it is unrealistic to assume steady wind conditions over a region
217 larger than shelf scale, hence computationally-expensive time-stepping methods would
218 be required to simulate swell waves. However, the model has generally reproduced the

219 magnitude and character of T_p throughout the year (Figure 4, Figure 6), considering such
220 uncertainties associated with rapid calculation methods.

4.3. Present-Day Benchmark Simulation

221 ECMWF-ERA-Interim reanalysis 3-hourly synoptic wind data described in section 3.2
222 were applied to lookup tables calculated for every cell of the shelf model grid. A benchmark
223 simulation was made for the entire ‘typical’ year 1993 when the annual NAO index was
224 closest to zero (0.12) for the available decade of wind data (Table 1). Outputs at all
225 time steps throughout 1993 were used to calculate the spatial distribution of annual rms
226 and peak H_s , T_p , and τ_w over the NW European shelf seas, considered as the benchmark
227 simulation (Figure 7).

4.4. Paleo Benchmark Simulation

228 Initially, a steady state SW wind (dominant wind direction over the NW European
229 shelf) of magnitude 22 m s^{-1} (typical gale wind speed) was applied over the entire model
230 domain for every 1 ka time slice from 12 ka BP to present. This identified key periods
231 when there were potentially large transitions in the wave climate over the NW European
232 shelf seas. From these pilot simulations, four paleo time slices were selected, in addition
233 to the present-day time slice described in section 4.3, for more detailed wave modeling:
234 12, 10, 8, and 6 ka BP. Using the paleobathymetries described in section 3.1, a series of
235 lookup tables were calculated for each paleo time slice, applying the same methodology
236 used for the present-day bathymetry case.

237 Climate model simulations [*Renssen et al.*, 2007] and proxy data on aeolian sand trans-
238 port [*Böse*, 1991] indicate that throughout the Holocene, wind directions over NW Europe

239 were generally similar to present-day wind directions. Therefore, the 3-hourly wind forc-
240 ing throughout 1993 was applied to each set of lookup tables corresponding to each of the
241 paleo time slices. The resulting paleowave climates for this ‘typical’ NAO year of wind
242 forcing were calculated (e.g. Figure 8) and contrasted with the present-day bathymetry
243 benchmark simulation. Anomalies in bed shear stress between all paleo simulations and
244 the present-day simulation are presented in Figure 9 (annual rms τ_w) and Figure 10 (an-
245 nual maximum τ_w). These paleowave model benchmark simulations therefore demonstrate
246 the influence of bathymetry on the resulting wave climate. Sensitivity of the model results
247 to variations in the wind forcing is investigated in section 6.

5. Model Results

248 Generally, the present-day annual mean wave climate over the NW European shelf seas
249 relates to fetch lengths associated with the predominantly southwesterly winds (Figure
250 7a,b). Therefore, in the exposed Celtic Sea, the Atlantic seaboard of Ireland and Scot-
251 land, and the northern and eastern North Sea, annual rms significant wave heights (H_s)
252 are of order 3 – 4 m, in contrast to 1 – 2 m in the relatively sheltered Irish Sea, English
253 Channel, and the UK seaboard of the North Sea. The corresponding peak annual H_s
254 for these exposed and sheltered regions are of order 10 – 15 m and 5 – 10 m, respec-
255 tively (Figure 7d). Annual rms T_p in exposed and sheltered regions of the shelf seas are
256 typically 7 – 8 s and 5 – 6 s, respectively (Figure 7b). Peak annual T_p in exposed and
257 sheltered regions are typically 18 – 19 s and 13 – 14 s, respectively (Figure 7e). Wave
258 height (and hence wave energy) at shelf scale is mainly a function of wind/wave expo-
259 sure and is largely independent of water depth. However, due to the attenuation of wave
260 orbital velocity with depth, bed shear stress is strongly related to water depth and the

261 level of exposure. Therefore, present-day annual rms wave-induced bed shear stresses are
262 greatest in the relatively shallow (water depths of order 30 – 40 m) regions of the North
263 Sea (Figure 7c), particularly Dogger Bank and the German Bight. In these regions, the
264 modest mean wave orbital motion available at the surface (Figure 7a) has a significant
265 influence on the bed since relatively little net attenuation occurs in such shallow water
266 depths. Annual rms bed shear stress in these regions is therefore relatively high - of order
267 $1 - 2 \text{ N m}^{-2}$. In contrast, wave motion is considerably attenuated at the bed in the deeper,
268 but more exposed, Celtic Sea and northern North Sea, leading to low annual rms values
269 of wave-induced bed shear stress - of order $0 - 0.5 \text{ N m}^{-2}$. The corresponding peak annual
270 bed shear stress in these shallow and deep regions is of order $5 - 10 \text{ N m}^{-2}$ and $0 - 2 \text{ N}$
271 m^{-2} , respectively.

272 In contrast to simulations which use the present-day bathymetry, results of the wave
273 model applied to the 12 ka BP bathymetry indicate that annual rms and peak annual
274 significant wave heights were reduced over the remaining ‘wet’ regions of the shelf seas
275 (Figure 8a,d). This decrease was due to shoaling and the reduction in fetch lengths
276 resulting from changes in relative sea level redefining the position of the coastline. In
277 the Celtic Sea, annual rms wave heights were relatively constant between 12 ka BP and
278 present (Figure 7a, Figure 8a), but in the northern North Sea, annual rms wave heights
279 were about 1 m lower at 12 ka BP. In the case of peak annual wave heights, in contrast
280 to the present-day wave climate, there was a decrease of order 3 – 4 m at 12 ka BP in
281 both the Celtic Sea and the northern North Sea (Figure 7d, Figure 8d). However, despite
282 a reduction in wave heights over the shelf seas at 12 ka BP, wave-induced bed shear
283 stresses were considerably higher at 12 ka BP, in contrast to the present-day. Since wave

284 orbital motion is attenuated with depth, at 12 ka BP there was an overall increase in wave
285 motion at the bed, and hence higher bed shear stress, over this shallower shelf. Annual
286 rms and peak annual bed shear stress at 12 ka BP are plotted in Figure 8c and Figure
287 8f, respectively, but the contrast between present-day bed shear stress is made clearer
288 in the anomaly plots of Figure 9 and Figure 10. These plots also contain information
289 at intermediate time slices 6, 8, and 10 ka BP. Generally, as sea levels rose over the
290 last 12,000 years, water depth over the shelf seas increased, accompanied by a reduction
291 in wave-induced bed shear stress. Beginning with the 12 ka BP time slice, annual rms
292 bed shear stresses were much higher than present in the Celtic Sea and northwest North
293 Sea (Figure 9d). In contrast, peak annual bed shear stress was significantly increased
294 in most regions of the shelf seas which were ‘wet’, particularly the Celtic Sea, exposed
295 Atlantic waters of Ireland and Scotland, and the northern North Sea (Figure 10d). At
296 10 ka BP, annual rms bed shear stresses were considerably higher than present in the
297 central northern North Sea (Figure 9c), whereas peak annual bed shear stress was again
298 significantly increased in most regions of the shelf seas (Figure 10c). At 8 ka BP (Figure
299 9b), annual rms bed shear stresses over Dogger Bank and in the German Bight were
300 significantly higher than present-day values. Due to shoaling, the peak annual bed shear
301 stresses in these relatively shallow regions remained similar to present-day values at this
302 time slice, whereas peak annual bed shear stress increased in both the northern North Sea
303 and the Celtic Sea (Figure 10b). Other than a slight increase in annual rms bed shear
304 stress over Dogger Bank, the results at 6 ka BP were generally similar to present-day
305 conditions (Figure 9a, Figure 10a), since relatively little change in sea level occurred over
306 the last 6000 years.

6. Sensitivity to Inter-Annual Variability in Wind Forcing

307 The results discussed in section 5 were based on the 3-hourly synoptic wind forcing
308 for 1993, applied to discrete time slices from 12 ka BP to present. Clearly, paleo wind
309 climates were different to present-day wind climates. However, wind predictions from
310 paleoclimate models [e.g. *Renssen et al.*, 2007] are not available for all our timeslices,
311 at the same high spatial/temporal resolution, for the same duration or validated to
312 the same extent as the ECMWF-ERA-Interim reanalysis data (see PMIP2 database -
313 <http://pmip2.lsce.ipsl.fr/pmip2/>). Therefore, in order to represent the variability in wind
314 climate over the NW European shelf seas during the last 12 ka, the model was run with
315 ECMWF-ERA-Interim reanalysis years in the decade 1989 – 1998. This decade contained
316 considerable variation in the NAO, with annual means ranging from -1.01 (1996) to 1.23
317 (1990) (Table 1). Thus, while we cannot force the model with observed or modelled
318 wind data from the different time slices, this range of years covers synoptic conditions
319 ranging from generally anticyclonic (more negative NAO), and so characteristically cold
320 and dry, to mostly strong westerlies (positive NAO), and warm and wet. This range of
321 conditions gives an estimate of the sensitivity of the wave heights and bed shear stress to
322 atmospheric forcing, and so enables identification of trends over time due to bathymetric
323 changes rather than atmospheric forcing.

324 The model results are presented as the annual rms and peak annual H_s (Figure 11) and
325 τ_w (Figure 12), averaged over two regions. The first averaging region (used to calculate
326 Figure 11a,b and Figure 12a,b) used only model cells which remained ‘wet’ continuously
327 over the last 12,000 years, i.e. the area used to compute these averages was fixed, regardless
328 of time slice. The second averaging region (used to calculate Figure 11c,d and Figure

329 12c,d) used only model cells with water depth $h < 100$ m at each time slice, i.e. this
330 averaging region varied between time slices. There is significant spread in the results
331 (Figure 11 and Figure 12), reflecting the inter-annual variability in wind forcing, but
332 two trends dominate. Whereas annual rms and peak annual wave heights progressively
333 increased over the NW European shelf seas during the last 12,000 years (Figure 11), wave-
334 induced bed shear stress progressively decreased over the same period (Figure 12). In the
335 region of the shelf seas which were continuously wet over the last 12,000 years, annual
336 rms H_s increased by around 20% over the last 12 ka (Figure 11a) and peak annual H_s
337 increased by around 40% (Figure 11b). In the same region, annual rms τ_w was reduced
338 by almost an order of magnitude from ~ 0.4 N m⁻² at 12 ka BP to 0.06 N m⁻² at 0 ka
339 BP (Figure 12a), while peak annual τ_w was reduced from 2 to 0.8 N m⁻² (Figure 12b).
340 Considering only water depths $h < 100$ m at each time slice, annual rms H_s increased
341 by around 15% over the last 12,000 years (Figure 11c) and peak annual H_s increased by
342 around 30% (Figure 11d). Using the same criteria for the averaging region at each time
343 slice ($h < 100$ m), annual rms τ_w was reduced from around 0.5 to 0.3 N m⁻² over the last
344 12,000 years (Figure 12c), while peak annual τ_w was reduced from 3 to 2.6 N m⁻² (Figure
345 12d).

7. Discussion

346 Over the last 12,000 years, annual rms and peak annual significant wave heights (H_s)
347 increased over the NW European shelf seas (Figure 11). This was primarily due to an
348 increase in relative sea levels through the Late-glacial and Holocene redefining the location
349 of the coastline, and hence progressively extending fetch lengths in most regions of the
350 shelf seas. This increase in wave heights is particularly noticeable in the northwestern

351 North Sea and the Irish Sea (Figure 7a,d and Figure 8a,d). However, regardless of this
 352 change in fetch length, peak annual wave heights also increased in many exposed regions
 353 such as the Celtic Sea. In the Celtic Sea, southwesterly winds are responsible for the
 354 largest waves. Since such waves are not fetch-limited, the increase in peak annual wave
 355 height from 12 ka BP to present in this region must be due to changes in relative water
 356 depth. For a given wave period T , wavelength L is related to water depth h through the
 357 dispersion relationship

$$358 \quad \sigma^2 = gk \tanh(kh) \quad (2)$$

359 where $\sigma = 2\pi/T$ is the angular frequency and $k = 2\pi/L$ is the wave number. Hence,
 360 wavelength (and therefore wave height) will increase with increasing water depth. There-
 361 fore, an increase in relative sea level through the Late-glacial and Holocene corresponds
 362 to an increase in peak wave heights in regions where the low-frequency waves are not
 363 fetch-limited, such as the Celtic Sea.

364 Over the last 12,000 years, annual rms and peak annual wave-induced bed shear stress
 365 (τ_w) decreased over the NW European shelf seas (Figure 12). This reduction in bed shear
 366 stress can largely be explained by increasing water depths through the Late-glacial and
 367 Holocene. Wave orbital velocities are at a maximum at the surface and attenuate with
 368 depth as a function of wavelength. Since the vertical component of velocity w is zero at
 369 the bed, it is the horizontal component of velocity u which is responsible for bed shear
 370 stress. The amplitude of u is attenuated with depth as

$$371 \quad u_0 = \frac{\pi H}{T} \left[\frac{\cosh(k(z+h))}{\sinh(kh)} \right] \quad (3)$$

372 This calculation at the bed is shown graphically in Figure 13 for a range of H and T ,
373 applied to a range of water depths h . The mean depth in the Celtic Sea is shown on the
374 plot at two different time slices: 12 ka and 0 ka BP. In the Celtic Sea, the annual rms
375 value of H_s at 12 ka BP was typically 2.25 m (Figure 11a), corresponding with a value
376 of $u_0 = 0.15 \text{ m s}^{-1}$, plotted as a filled triangle in Figure 13. At 0 ka BP, annual rms H_s
377 increased to 2.75 m in the Celtic Sea, corresponding with a negligible value of $u_0 = 0.002$
378 m s^{-1} , plotted as a filled circle in Figure 13. Therefore, despite a 0.5 m increase in annual
379 rms H_s over the last 12,000 years, the amplitude of horizontal particle velocity at the bed
380 was reduced by two orders of magnitude in the Celtic Sea. Since τ_w is a function of u_0^2 ,
381 bed shear stress in this region will be reduced by several orders of magnitude.

382 The increase in wave height in the southern North Sea over the last 8000 years is consis-
383 tent with the findings of other studies [e.g. *Beets et al.*, 1992; *van der Molen and de Swart*,
384 2001a]. This gives confidence in the results of the present study, which has extended these
385 calculations back to 12 ka BP (Figure 11) and over a much larger geographical area. In
386 terms of wave-effects at the bed, previous model studies of the southern North Sea have
387 demonstrated that the magnitude of wave-induced bed load transport decreased through
388 the Holocene [*van der Molen and de Swart*, 2001a]. In addition, numerical and seismic
389 studies in the Celtic Sea have indicated that tidal and wave erosion at the top of sand
390 banks is at present much weaker than during the early Holocene [*Belderson et al.*, 1986;
391 *Reynaud et al.*, 1999]. Again, these published results are consistent with the findings of
392 the present study (Figure 12) which apply to a larger geographic region.

393 It was suggested in section 1 that the shelf-scale ratio between wave- and tidal-induced
394 bed shear stress will have varied considerably over the Late-glacial and Holocene due to

395 changes in water depth. Wave-induced bed shear stress is considerably more sensitive
 396 to changes in water depth than tidal-induced bed shear stress. Here we introduce mean
 397 tidal-induced stress τ_0 in terms of quadratic bottom drag by using paleotidal model output
 398 from *Uehara et al.* [2006] as

$$399 \quad \tau_0 = \rho C_D \overline{U_{M_2}^2} \quad (4)$$

400 where $\rho = 1023 \text{ kg m}^{-3}$ is the density of seawater, $C_D = 0.0026$ is the drag coefficient and
 401 $\overline{U_{M_2}^2}$ is the square of the M_2 tidal current averaged over a tidal cycle. The instantaneous
 402 velocities u and v in an ellipse can be written as

$$403 \quad u = U_{maj} \cos(\omega t) \quad \text{and} \quad v = U_{min} \sin(\omega t) \quad (5)$$

404 where u and v are velocity components along major and minor axes of the ellipse, U_{maj}
 405 and U_{min} are the semi-major and semi-minor axes of the M_2 tidal current ellipses and ω
 406 is the angular frequency. Therefore, the square of the tidal current averaged over a tidal
 407 cycle is

$$408 \quad \begin{aligned} \overline{U^2} &= U_{maj}^2 \overline{\cos^2(\omega t)} + U_{min}^2 \overline{\sin^2(\omega t)} \\ 409 \quad &= \frac{1}{2}(U_{maj}^2 + U_{min}^2) \end{aligned} \quad (6)$$

410 Hence, equation 4 can be written as

$$411 \quad \tau_0 = \frac{1}{2} \rho C_D (U_{maj}^2 + U_{min}^2) \quad (7)$$

412 By combining values of τ_0 with the results of the present study, variations in the spatial
 413 distribution of the ratio τ_w/τ_0 over the Late-glacial and Holocene can be quantified for the
 414 NW European shelf seas (Figure 14). It is to be noted that this ratio compares the wave-
 415 induced bed shear stress with bed shear stress generated by only the M_2 tidal currents.

416 In reality, the ratio τ_w/τ_0 will be lower, due to the addition of further tidal constituents.
417 However, at 12 ka BP waves generally dominated bed shear stress in the northwest North
418 Sea (Figure 14e). At present, waves generally dominate over Dogger Bank and the eastern
419 North Sea (Figure 14a). By making use of the two averaging regions described in section 6,
420 shelf-scale variations in mean tidal-induced bed shear stress (τ_0) over the last 12,000 years
421 are plotted, along with variations in the annual rms wave-induced bed shear stress (τ_w)
422 (Figure 15a,c). Over the region of the shelf seas which remained wet continuously over the
423 last 12,000 years, the ratio $\tau_w/\tau_0 \approx 1$ at 12 ka BP (Figure 15b). This ratio reduced over
424 the last 12,000 years in this fixed region to its present-day estimate of $\tau_w/\tau_0 = 0.5$. Since
425 these calculations are for a region which is fixed, regardless of changes in water depth at
426 each time slice, it is also useful to compare the ratio τ_w/τ_0 for only regions of the shelf seas
427 with water depths $h < 100$ m at each time slice. In this case, the ratio τ_w/τ_0 remained
428 close to 1 over the last 12,000 years (Figure 15d). However, there was an anomaly at 8
429 ka BP when $\tau_w/\tau_0 \approx 1.7$, due to a relatively large reduction in τ_0 at this time slice. This
430 anomaly is also present, but not as prominent, in the fixed averaging region (Figure 15b).
431 The global tidal model of *Uehara et al.* [2006] demonstrates that in the period between
432 the LGM and present, the minimum value of global tidal dissipation rate occurred at 8
433 ka BP. It is to be noted that mean τ_0 (Figure 15a,c) was smaller than peak τ_w (Figure
434 12b,d) at all time slices, indicating the larger impact of wave processes than tidal effects
435 during storm events throughout the Late-glacial and Holocene.

436 Although the trend of decreasing τ_w through the Late-glacial and Holocene is clear
437 (Figure 12), there is considerable spread in the results when considering inter-annual
438 variability in wind forcing (Table 1). In addition, although the range of inter-annual

439 variability of peak annual τ_w in the fixed averaging region (model cells which were wet
440 continuously from 12 ka BP to present) remained approximately constant over the last
441 12,000 years (Figure 12b), there was a considerable reduction in the range of inter-annual
442 variability in annual rms τ_w over the last 12,000 years in the same region (Figure 12a).
443 Increased inter-annual variability in annual rms τ_w at 12 ka BP can be explained with
444 reference to the Celtic Sea. For typical water depths in the Celtic Sea at 12 ka BP, the
445 mean annual wave climate corresponds with an amplitude of horizontal particle velocity
446 at the bed $u_0 = 0.15 \text{ m s}^{-1}$ (filled triangle on Figure 13). This has reduced considerably
447 to its present-day value of $u_0 = 0.002 \text{ m s}^{-1}$ (filled circle on Figure 13), despite a 0.5
448 m increase in annual rms wave height. Since inter-annual variability of annual rms wave
449 heights has been relatively constant over the last 12,000 years (Figure 11), it is clear from
450 Figure 13 that for a fixed range of variability in H_s , variability of u_0 (and hence τ_w) will
451 be considerably greater at $h = 30 \text{ m}$ (representing the 12 ka BP time slice), compared
452 with $h = 100 \text{ m}$ (representing the present-day time slice). This explains the greater inter-
453 annual variability of τ_w at 12 ka BP compared to 0 ka BP on Figure 12a. There is little
454 change in the inter-annual variability of peak annual τ_w over the last 12,000 years (e.g.
455 Figure 12b) since the annual peak at any location is generally due to a single annual
456 ‘extreme’ event, located towards the right-hand-side of Figure 13, and therefore due to a
457 narrow range of wind/wave conditions.

8. Conclusions

458 Using the present-day bathymetry of the NW European shelf seas, a wave model was
459 first validated using high resolution data from a series of wave buoys. Applying a decade
460 of 3-hourly wind fields, the model was then applied to a series of paleobathymetries, to

461 contrast wave climates of the NW European shelf seas for time slices 12, 10, 8, 6, and 0
462 ka BP. Model results demonstrated that wave heights increased through the Late-glacial
463 and Holocene in regions of the shelf seas which were wet continuously over this time
464 period. This increase in wave height was a consequence of increases in fetch length due
465 to changes in relative sea level redefining the position of the coastline for successive time
466 slices. This increase in wave height was accompanied by a large reduction in the annual
467 rms wave-induced bed shear stress, primarily due to a reduction in the magnitude of wave
468 orbital velocity penetrating to the bed for increasing relative sea level. Comparison of
469 wave model output with results of a previous paleotidal model study over the same study
470 area demonstrated significant changes in the spatial distribution of the ratio of annual
471 rms wave- to tidal-induced bed shear stress over the last 12,000 years. In regions of the
472 shelf seas which remained wet continuously over the last 12,000 years, the annual mean
473 ratio of wave- to (M_2) tidal-induced bed shear stress decreased from 1 (at 12 ka BP) to
474 its present day value of 0.5. Therefore, compared to present-day conditions, waves had a
475 more important contribution to large-scale sediment transport processes in the Celtic Sea
476 and the northwestern North Sea at 12 ka BP.

477 **Acknowledgments.** The paleobathymetry data were provided by Kurt Lambeck, Aus-
478 tralian National University. The 3-hourly synoptic wind data were provided by the Euro-
479 pean Centre for Medium-Range Weather Forecasts (ECMWF) and hourly time series of
480 wind data from meteorological stations around the UK provided by the UK Met Office.
481 Wave buoy data were provided by the UK Centre for Environment, Fisheries and Aqua-
482 culture Science (CEFAS) and the British Oceanographic Data Centre (BODC). NAO data
483 are publicly available from Tim Osborn, University of East Anglia. The authors would also

484 like to thank two anonymous reviewers for their constructive comments. James Scourse
485 acknowledges the support of a Royal Society-Leverhulme Trust Senior Research Fellow-
486 ship. Simon Neill acknowledges the support of the Higher Education Funding Council for
487 Wales and the Welsh Assembly Government.

References

- 488 Austin, R. M., Modelling Holocene tides on the NW European continental shelf, *Terra*
489 *Nova*, 3, 276–288, 1991.
- 490 Barrow, E., and M. Hulme, Describing the surface climate of the British Isles, in *Climates*
491 *of the British Isles*, edited by M. Hulme and E. Barrow, pp. 33–62, Routledge, London,
492 1997.
- 493 Beets, D. J., L. van der Valk, and M. J. F. Stive, Holocene evolution of the coast of
494 Holland, *Mar. Geol.*, 103, 423–443, 1992.
- 495 Belderson, R. H., R. D. Pingree, and D. K. Griffiths, Low sea-level tidal origin of Celtic
496 Sea sand banks - evidence from numerical modelling of M₂ tidal streams, *Mar. Geol.*,
497 73, 99–108, 1986.
- 498 Berger, A., M. F. Loutre, and J. Laskar, Stability of the astronomical frequencies over the
499 Earth's history for paleoclimate studies, *Science*, 255, 560–566, 1992.
- 500 Booij, N., R. C. Ris, and L. H. Holthuijsen, A third-generation wave model for coastal
501 regions - 1. model description and validation, *J. Geophys. Res.*, 104, 7649–7666, 1999.
- 502 Böse, M., A palaeoclimatic interpretation of frost-wedge casts and aeolian sand deposits
503 in the lowlands between Rhine and Vistula in the upper Pleniglacial and Late Glacial,
504 *Z. Geomorphol., Suppl. Band 90*, 15–28, 1991.

- 505 Boulton, G. S., G. D. Smith, A. D. Jones, and J. Newsome, Glacial geology and glaciology
506 of the last mid-latitude ice sheets, *J. Geol. Soc. London*, *142*, 447–474, 1985.
- 507 Cameron, T. D. J., M. S. Stoker, and D. Long, The history of Quaternary sedimentation
508 in the UK sector of the North Sea Basin, *J. Geol. Soc. London*, *144*, 43–58, 1987.
- 509 Carr, S. J., R. Holmes, J. J. M. van der Meer, and J. Rose, The Last Glacial Maximum
510 in the North Sea Basin: micromorphological evidence of extensive glaciation, *J. Quat.*
511 *Sci.*, *21*, 131–153, 2006.
- 512 Carter, D. J. T., Prediction of wave height and period for a constant wind velocity using
513 the JONSWAP results, *Ocean Eng.*, *9*, 17–33, 1982.
- 514 Draper, L., Wave climatology of the U.K. continental shelf, in *The north-west European*
515 *shelf seas: the sea bed and the sea in motion. II. Physical and chemical oceanography,*
516 *and physical resources*, edited by F. T. Banner, M. B. Collins, and K. S. Massie, pp.
517 353–368, Elsevier, 1980.
- 518 Elliott, A. J., and S. P. Neill, Simulating storm waves in the Irish Sea, *Proceedings of the*
519 *Institution of Civil Engineers - Maritime Engineering*, *160*, 57–64, 2007.
- 520 Hinton, A. C., Holocene tides of The Wash, U.K.: the influence of water-depth and
521 coastline-shape changes on the record of sea-level change, *Mar. Geol.*, *124*, 87–111,
522 1995.
- 523 Hinton, A. C., Tides in the northeast Atlantic: considerations for modelling water depth
524 changes, *Quat. Sci. Rev.*, *15*, 873–894, 1996.
- 525 Hurrell, J. W., and H. van Loon, Decadal variations in climate associated with the north
526 Atlantic oscillation, *Clim. Change*, *36*, 301–326, 1997.

- 527 Komen, G. J., L. Cavaleri, M. Donelan, K. Hasselmann, S. Hasselmann, and P. A. E. M.
528 Janssen, *Dynamics and Modelling of Ocean Waves*, Cambridge University Press, 1994.
- 529 Lambeck, K., Late Devensian and Holocene shorelines of the British Isles and North
530 Sea from models of glacio-hydro-isostatic rebound, *J. Geol. Soc. London*, *152*, 437–448,
531 1995.
- 532 Lambeck, K., and J. Chappell, Sea level change through the last glacial cycle, *Science*,
533 *292*, 679–686, 2001.
- 534 Lambeck, K., and A. Purcell, Sea-level change in the Irish Sea since the Last Glacial
535 Maximum: constraints from isostatic modelling, *J. Quat. Sci.*, *16*, 497–506, 2001.
- 536 Lambeck, K., A. Purcell, P. Johnston, M. Nakada, and Y. Yokoyama, Water-load def-
537 inition in the glacio-hydro-isostatic sea-level equation, *Quat. Sci. Rev.*, *22*, 309–318,
538 2003.
- 539 Milne, G. A., J. X. Mitrovica, and D. P. Schrag, Estimating past continental ice volume
540 from sea-level data, *Quat. Sci. Rev.*, *21*, 361–376, 2002.
- 541 Mitrovica, J. X., M. E. Tamisea, J. L. Davis, and G. A. Milne, Recent mass balance of
542 polar ice sheets inferred from patterns of global sea-level change, *Nature*, *409*, 1026–
543 1029, 2001.
- 544 Neill, S. P., M. R. Hashemi, and A. J. Elliott, An enhanced depth-averaged tidal model for
545 morphological studies in the presence of rotary currents, *Cont. Shelf Res.*, *27*, 82–102,
546 2007.
- 547 Neill, S. P., A. J. Elliott, and M. R. Hashemi, A model of inter-annual variability in beach
548 levels, *Cont. Shelf Res.*, *28*, 1769–1781, 2008.

- 549 Newell, N. D., Recent terraces of tropical limestone shores, *Z. Geomorphol., Suppl. Band*
550 *3*, 87–106, 1961.
- 551 Ogston, A. S., and R. W. Sternberg, Sediment-transport events on the northern California
552 continental shelf, *Mar. Geol.*, *154*, 69–82, 1999.
- 553 Palutikof, J., T. Holt, and A. Skellern, Wind: resources and hazard, in *Climates of the*
554 *British Isles*, edited by M. Hulme and E. Barrow, pp. 220–242, Routledge, London,
555 1997.
- 556 Peltier, W. R., Ice-age paleotopography, *Science*, *265*, 195–201, 1994.
- 557 Peltier, W. R., On eustatic sea level history: Last Glacial Maximum to Holocene, *Quat.*
558 *Sci. Rev.*, *21*, 377–396, 2002.
- 559 Pingree, R. D., and D. K. Griffiths, Sand transport paths around the British Isles resulting
560 from the M_2 and M_4 tidal interactions, *J. Mar. Biol. Assoc. U.K.*, *59*, 497–513, 1979.
- 561 Renssen, H., C. Kasse, J. Vandenberghe, and S. J. Lorenz, Weichselian Late Pleniglacial
562 surface winds over northwest and central Europe: a model–data comparison, *J. Quat.*
563 *Sci.*, *22*, 281–293, 2007.
- 564 Reynaud, J.-Y., B. Tessier, S. Berné, H. Chamley, and M. Debatist, Tide and wave
565 dynamics on a sand bank from the deep shelf of the Western Channel approaches,
566 *Mar. Geol.*, *161*, 339–359, 1999.
- 567 Rippeth, T. P., J. D. Scourse, K. Uehara, and S. McKeown, Impact of sea-level rise
568 over the last deglacial transition on the strength of the continental shelf CO_2 pump,
569 *Geophys. Res. Lett.*, *35*, L24,604, 2008.
- 570 Ris, R. C., L. H. Holthuijsen, and N. Booij, A third-generation wave model for coastal
571 regions - 2. verification, *J. Geophys. Res.*, *104*, 7667–7681, 1999.

- 572 Scourse, J. D., K. Uehara, and A. Wainwright, Celtic Sea linear tidal sand ridges, the
573 Irish Sea Ice Stream and the Fleuve Manche: palaeotidal modelling of a transitional
574 passive margin depositional system, *Mar. Geol.*, *259*, 102–111, 2009.
- 575 Simmons, A., S. Uppala, D. Dee, and S. Kobayashi, ERA-Interim: new ECMWF re-
576 analysis products from 1989 onwards, *ECMWF Newsletter*, *110*, 25–35, 2006.
- 577 Uehara, K., J. D. Scourse, K. J. Horsburgh, K. Lambeck, and A. P. Purcell, Tidal evolution
578 of the northwest European shelf seas from the Last Glacial Maximum to the present,
579 *J. Geophys. Res.*, *111*, C09,025, 2006.
- 580 van der Molen, J., The influence of tides, wind and waves on the net sand transport in
581 the North Sea, *Cont. Shelf Res.*, *22*, 2739–2762, 2002.
- 582 van der Molen, J., and H. E. de Swart, Holocene wave conditions and wave-induced sand
583 transport in the southern North Sea, *Cont. Shelf Res.*, *21*, 1723–1749, 2001a.
- 584 van der Molen, J., and H. E. de Swart, Holocene tidal conditions and tide-induced sand
585 transport in the southern North Sea, *J. Geophys. Res.*, *106*, 9339–9362, 2001b.
- 586 Vincent, C. E., A. Stolk, and C. F. C. Porter, Sand suspension and transport on the
587 Middelkerke Bank (southern North Sea) by storms and tidal currents, *Mar. Geol.*, *150*,
588 113–129, 1998.

TABLE CAPTIONS

⁵⁸⁹ **Table 1.** Annual North Atlantic Oscillation (NAO) index, 1989-1998.

⁵⁹⁰ **Table 2.** Details of wave buoys and corresponding meteorological stations used for model vali-
⁵⁹¹ dation. Validation year was 2007 for all stations, except for Stevenson (1975).

FIGURE CAPTIONS

592 **Figure 1.** Bathymetry and coastline of present-day model domain. The dashed line, drawn at
593 a distance of 400 km from the model boundary, represents the fetch length for a fully developed
594 sea, based on the maximum modeled wind speed (30 m s^{-1} - violent storm) and a JONSWAP
595 spectrum. Since the model is not nested within a larger area wave model, model results outside
596 this dashed line were discarded. Asterisks show locations of six wave buoys (labeled) used for
597 model validation: LB=Liverpool Bay, SW=Scarweather, PB=Poole Bay, WG=West Gabbard,
598 TT=Tyne/Tees, and ST=Stevenson. Contours are water depth in meters, relative to mean sea
599 level.

600 **Figure 2.** Paleobathymetries for selected time slices. Contours are water depth in meters, rela-
601 tive to mean sea level. Grey shading represents land at each time slice. For reference, thick solid
602 line shows position of present-day coastline. (a) 6 ka BP, (b) 8 ka BP, (c) 10 ka BP, and (d) 12
603 ka BP.

604 **Figure 3.** Agreement between H_s measured at six wave buoys and H_s modeled by SWAN for one
605 year of simulation. The same year of simulation (2007) was used for all validation stations except
606 for Stevenson (1975). Details of the wave buoys are given in Table 2 and locations plotted in
607 Figure 1. (a) Liverpool Bay, (b) Scarweather, (c) Poole Bay, (d) West Gabbard, (e) Tyne/Tees,
608 and (f) Stevenson.

609 **Figure 4.** As in Figure 3, but for T_p .

610 **Figure 5.** Agreement between modeled and observed H_s shown as probability density plots.

611 Note that the in situ data for Stevenson is at coarser temporal resolution (3-hourly), and wind
 612 direction and magnitude are recorded in discrete intervals of 10° and 0.5 m s^{-1} , respectively;
 613 hence the change in resolution and horizontal banding in (f). Also shown is the equality line
 614 (dashed) at 45° . Color scale is percentage probability. (a) Liverpool Bay, (b) Scarweather, (c)
 615 Poole Bay, (d) West Gabbard, (e) Tyne/Tees, and (f) Stevenson.

616 **Figure 6.** As in Figure 5, but for T_p .

617 **Figure 7.** Annual (1993) rms and peak annual H_s , T_p and τ_w calculated at each model cell
 618 for present-day simulation using spatially-varying 3-hourly wind fields. (a) annual rms H_s , (b)
 619 annual rms T_p , (c) annual rms τ_w , (d) peak annual H_s , (e) peak annual T_p , and (f) peak annual
 620 τ_w .

621 **Figure 8.** Annual rms and peak annual H_s , T_p and τ_w calculated at each model cell for 12 ka BP
 622 time slice using spatially-varying 3-hourly wind fields for 1993. (a) annual rms H_s , (b) annual
 623 rms T_p , (c) annual rms τ_w , (d) peak annual H_s , (e) peak annual T_p , and (f) peak annual τ_w .

624 **Figure 9.** Anomaly in annual rms τ_w between paleo and present-day bathymetry simulations
 625 using 1993 wind data. (a) 6 ka BP, (b) 8 ka BP, (c) 10 ka BP, and (d) 12 ka BP.

626 **Figure 10.** As in Figure 9, but for peak annual τ_w .

627 **Figure 11.** Variation in spatially-averaged annual rms and peak annual H_s for modeled time
 628 slices from 12 ka BP until present. In (a) and (b), the region used for averaging is fixed, using
 629 only model cells which remained ‘wet’ continuously from 12 ka BP to present, and hence does not
 630 vary in size for averaging applied to each time slice. In (c) and (d), values are averaged over only

631 model cells with water depth $h < 100$ m, and hence the averaging region varies between time
 632 slices. The solid line indicates the results averaged for all years of wind forcing (1989 – 1998)
 633 and grey shading indicates the range of variability within this decade of wind forcing. (a) annual
 634 rms H_s (fixed area), (b) peak annual H_s (fixed area), (c) annual rms H_s ($h < 100$ m), and (d)
 635 peak annual H_s ($h < 100$ m).

636 **Figure 12.** As in Figure 11, but for annual rms and peak annual τ_w . (a) annual rms τ_w (fixed
 637 area), (b) peak annual τ_w (fixed area), (c) annual rms τ_w ($h < 100$ m), and (d) peak annual τ_w
 638 ($h < 100$ m).

639 **Figure 13.** Contoured amplitude of horizontal particle velocity u_0 (m s^{-1}) close to the bed for a
 640 range of water depths and wave conditions, calculated using equation 3. Horizontal dashed lines
 641 indicate mean water depths in the Celtic Sea at 12 ka and 0 ka BP. Where these lines intersect
 642 with vertical dashed lines indicates values of u_0 associated with mean annual wave conditions in
 643 the Celtic Sea at 12 ka BP (filled triangle) and 0 ka BP (filled circle).

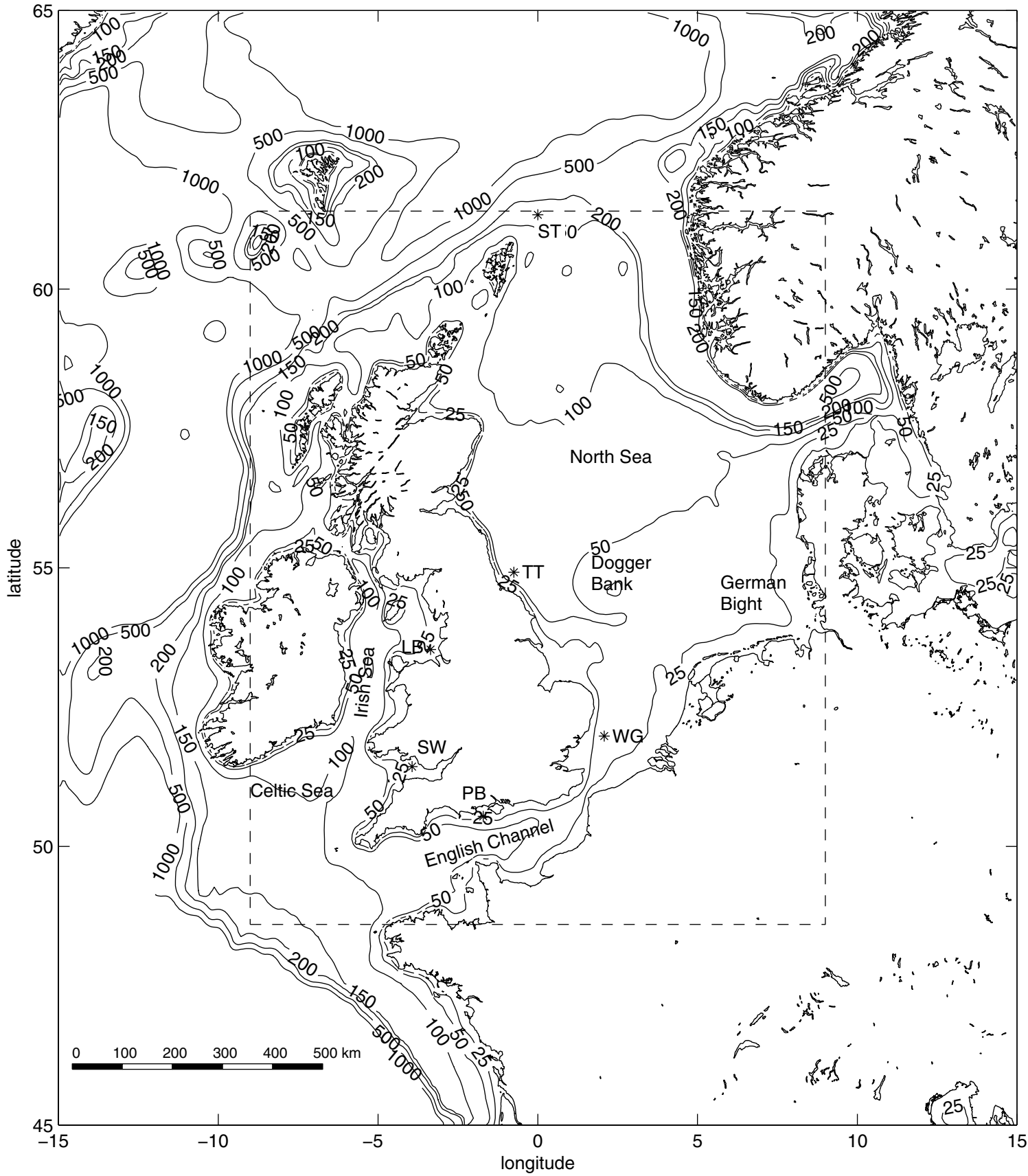
644 **Figure 14.** Spatial distribution of annual mean ratio τ_w/τ_0 for present-day and paleo simulations
 645 forced with 1993 wind data. (a) 0 ka BP, (b) 6 ka BP, (c) 8 ka BP, (d) 10 ka BP, and (e) 12 ka
 646 BP.

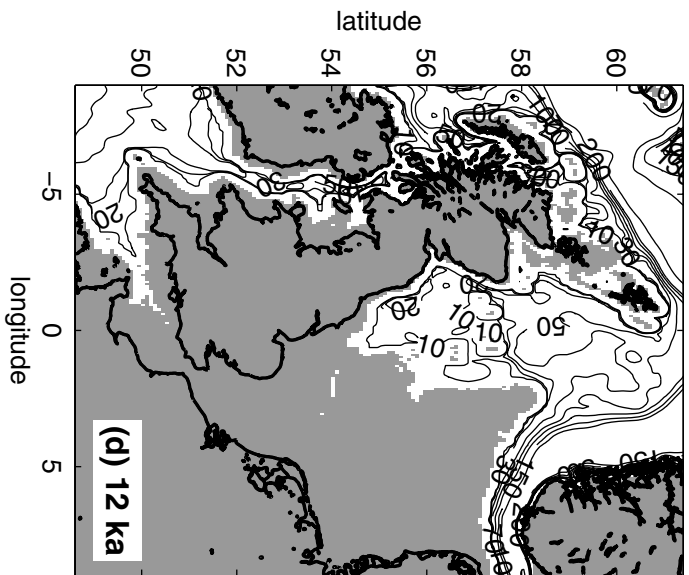
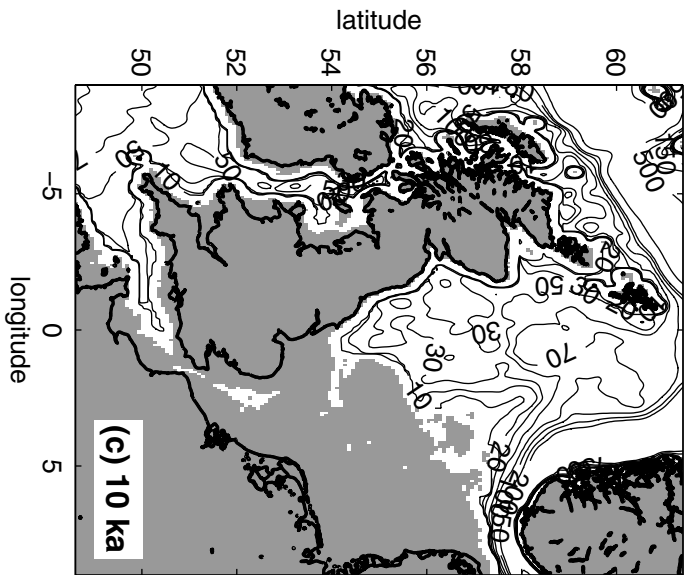
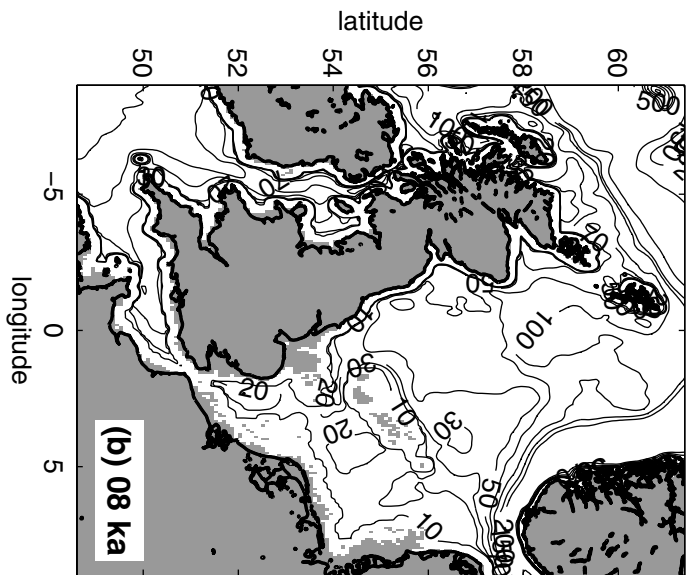
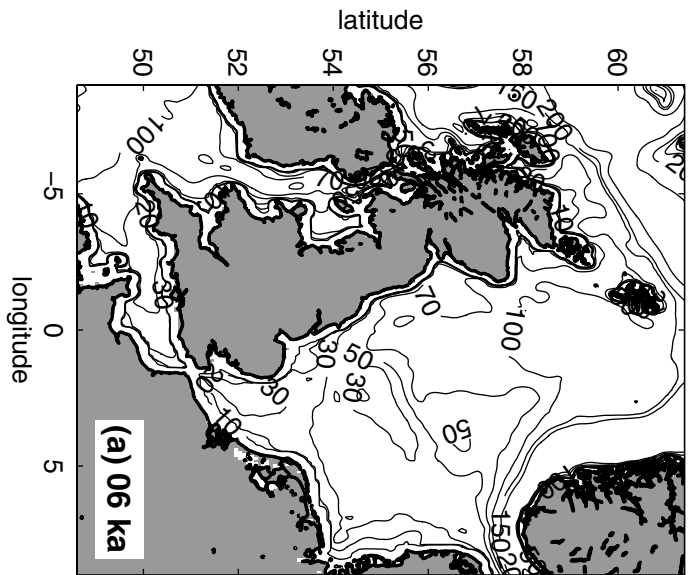
647 **Figure 15.** Comparison between annual rms wave- and tidal-induced bed shear stress for mod-
 648 eled time slices from 12 ka BP until present. In (a) and (b), the region used for averaging is
 649 fixed, using only model cells which remained ‘wet’ continuously from 12 ka BP to present, and
 650 hence does not vary in size for averaging applied to each time slice. In (c) and (d), values are
 651 averaged over only model cells with water depth $h < 100$ m, and hence the averaging region

652 varies between time slices. In (b) and (d), the solid line indicates the mean ratio τ_w/τ_0 for all
653 years of wind forcing (1989 – 1998), and grey shading indicates the range of variability within
654 this decade of wind forcing. (a) Annual rms τ_w and τ_0 (fixed area), (b) annual ratio τ_w/τ_0 (fixed
655 area), (c) annual rms τ_w and τ_0 ($h < 100$ m), and (d) annual ratio τ_w/τ_0 ($h < 100$ m).

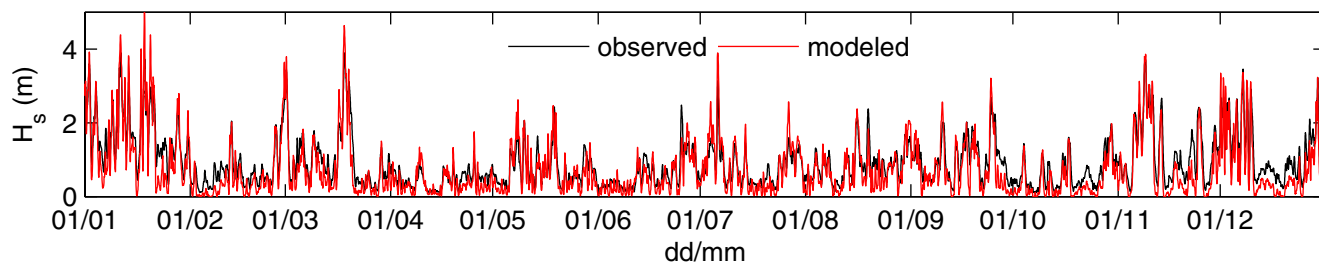
Year	NAO index
1989	0.57
1990	1.23
1991	0.34
1992	1.11
1993	0.12
1994	0.51
1995	-0.61
1996	-1.01
1997	-0.18
1998	0.25

Name of wave buoy	Latitude	Longitude	Water depth (m)	Corresponding station	Met.
Liverpool Bay	53°32'.05N	03°21'.20W	22	Crosby	
Scarweather	51°26'.00N	03°56'.00W	30	Milford Haven	
Poole Bay	50°38'.11N	01°43'.03W	26	Isle of Portland	
West Gabbard	51°58'.80N	02°04'.76E	34	Wattisham	
Tyne/Tees	54°55'.10N	00°44'.85W	65	Loftus	
Stevenson	61°20'.00N	00°00'.00E	160	Stevenson	

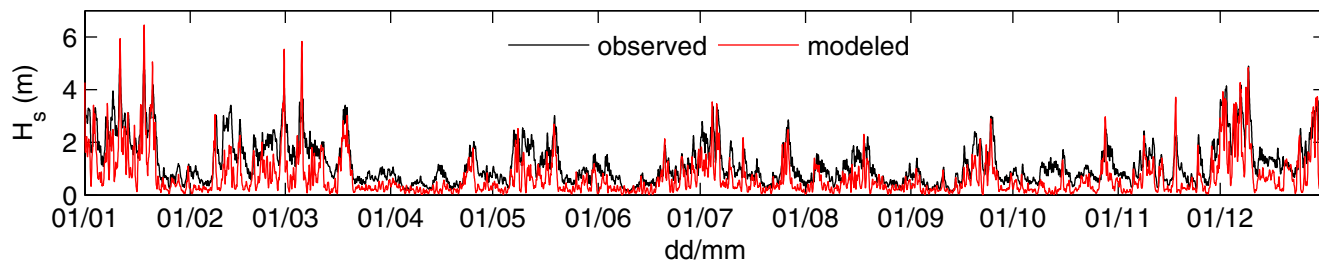




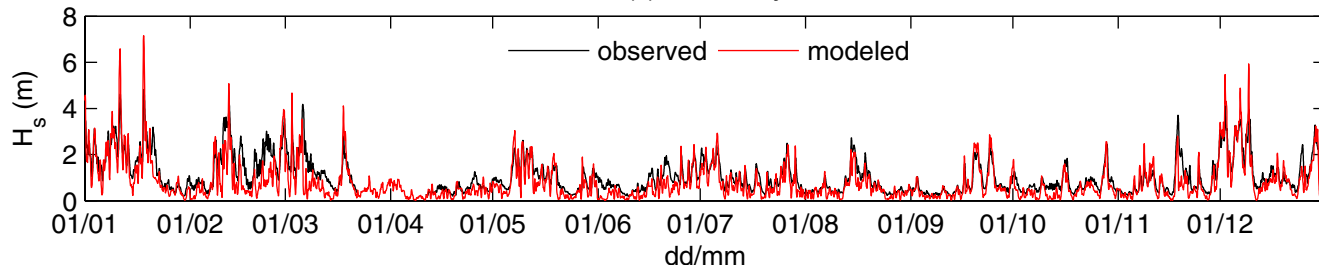
(a) Liverpool Bay



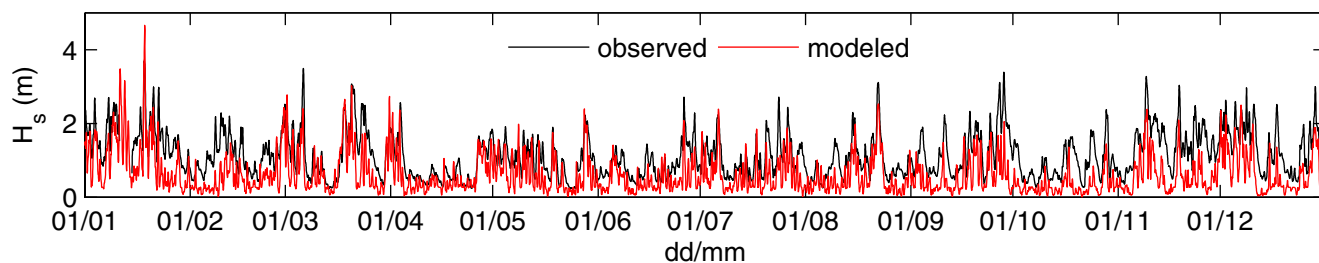
(b) Scarweather



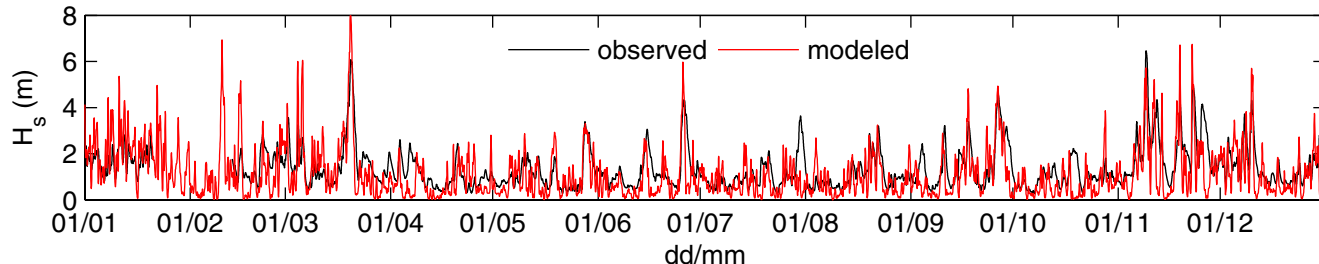
(c) Poole Bay



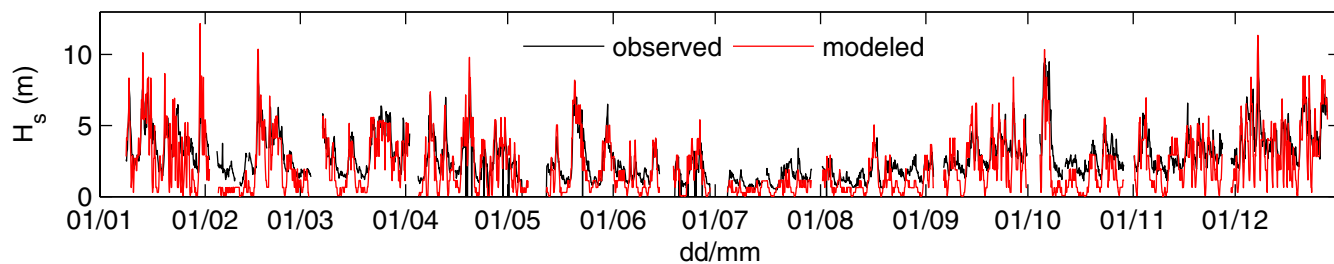
(d) West Gabbard



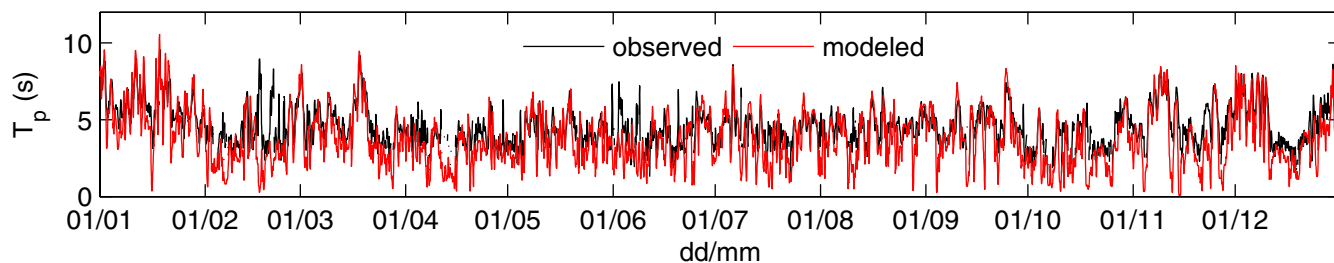
(e) Tyne/Tees



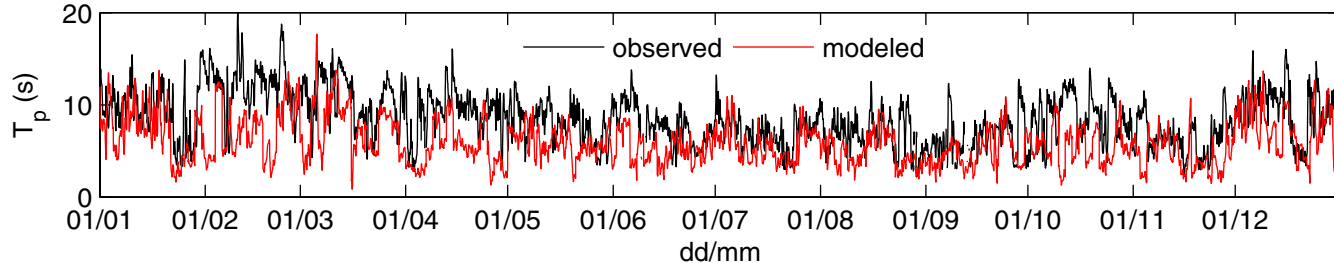
(f) Stevenson



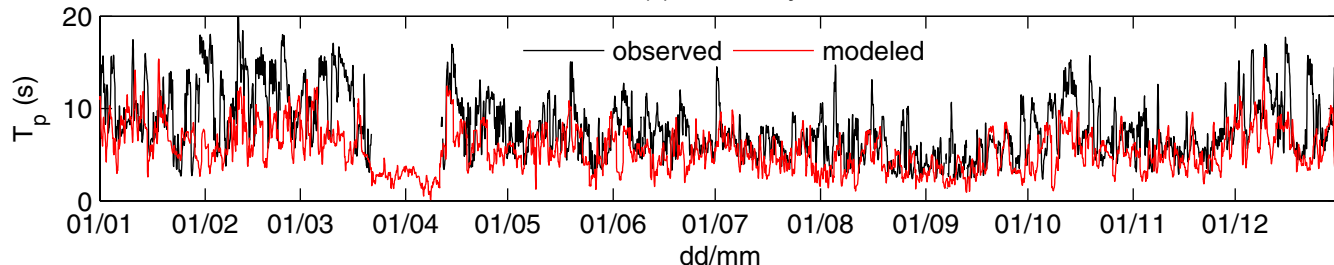
(a) Liverpool Bay



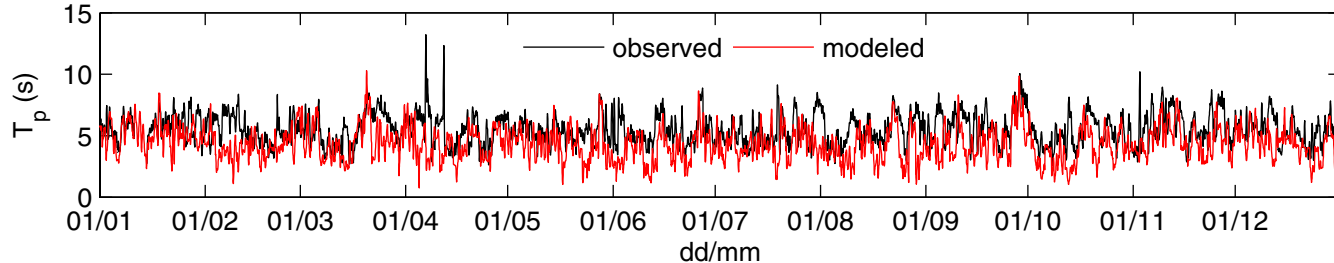
(b) Scarweather



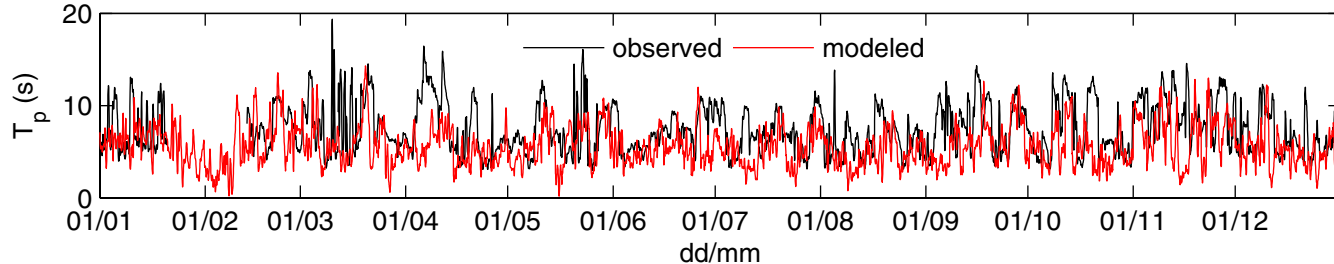
(c) Poole Bay



(d) West Gabbard



(e) Tyne/Tees



(f) Stevenson

